

Atom Probe Field-Ion Microscopy Characterization of Nickel and Titanium Aluminides

D. J. Larson and M. K. Miller

*Microscopy and Microanalytical Sciences Group, Metals and Ceramics Division,
Oak Ridge National Laboratory, Oak Ridge, TN 37831-6376*

A review of the contributions of atom probe field-ion microscopy to the characterization of nickel and titanium aluminides is presented. The nickel aluminide systems studied include boron-doped Ni₃Al and boron-, carbon-, beryllium-, zirconium-, molybdenum-, and hafnium-doped NiAl. These systems have been characterized in terms of solute segregation to boundaries, dislocations, and other defects, matrix solubilities, precipitation, and site-occupation probabilities. The partitioning behavior of impurities and alloying additions, matrix solubilities, precipitate compositions, and interfacial segregation in several of $\alpha_2 + \gamma$ titanium aluminides and related alloys are also reviewed. Published by Elsevier Science Inc.

INTRODUCTION

Many different types of intermetallic compounds have been the focus of atom probe field-ion microscope (APFIM) characterizations. The majority of the systematic studies have concentrated on nickel and titanium aluminides due to their potential high-temperature applications. Most of these characterizations have studied the role of microalloying additions that were added to the intermetallic compound to improve the properties. Atom probe investigations have provided information on the solute segregation to boundaries, inter-phase interfaces and defects, clustering and precipitation, and solute partitioning between the phases present. The APFIM is well suited to the characterization of the segregation and partitioning behavior of the microalloying elements in the microstructure due to its near atomic spatial resolution, light element sensitivity, high mass resolution, and low detection levels [1, 2]. It should be noted that in addition to the studies included in this review, other inter-

metallic compounds have been characterized, and additional intermetallic phases have been studied in other alloys, for example γ' and γ'' precipitates in nickel-based superalloys. A review of these APFIM studies may be found elsewhere [1].

NICKEL ALUMINIDES

A variety of microalloying elements have been used to improve the mechanical properties of polycrystalline Ni₃Al and NiAl [3]. Boron additions of as little as 200 atomic ppm to the L₁₂-ordered Ni₃Al produce dramatic improvements in ductility [4, 5]. However, boron additions to the B₂-ordered NiAl have a significantly different effect on the microstructure and the mechanical properties [6]. Although additions of as little as 20 atomic ppm of boron improve the ductility, larger amounts significantly increase the yield strength. Zirconium additions have also been shown to be beneficial to the mechanical properties of NiAl. The fracture mode has been shown to change

from an intergranular to a mixed transgranular and intergranular mode in zirconium-doped NiAl [7]. Molybdenum additions of between 0.4 and 1.6at.% Mo to NiAl have also been shown to significantly improve the room temperature ductility and high-temperature yield strength [8]. (Note that atomic percent will be used through this paper unless otherwise noted.)

BORON ADDITIONS TO Ni₃Al

Miller and Horton were the first to demonstrate that boron additions in Ni₃Al segregate to antiphase, twin, and grain boundaries [9]. Subsequent atom probe investigations have revealed that boron segregates to all defects in the alloy [9–16]. Examples of a boron-decorated grain boundary and an antiphase boundary in Ni₃Al are shown in Fig. 1. The boundaries shown in these field ion micrographs are decorated with brightly imaging spots. The unique single-atom identification capability of the atom probe was used to determine that these brightly imaging spots were boron atoms [1]. Field ion micrographs of two different grain boundaries, shown in Fig. 2, re-

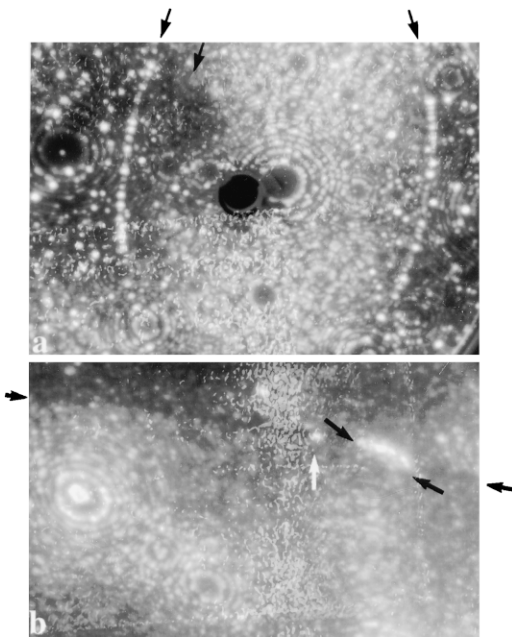


FIG. 1. Field ion micrographs of (a) antiphase, and (b) grain boundaries in boron-doped Ni₃Al.

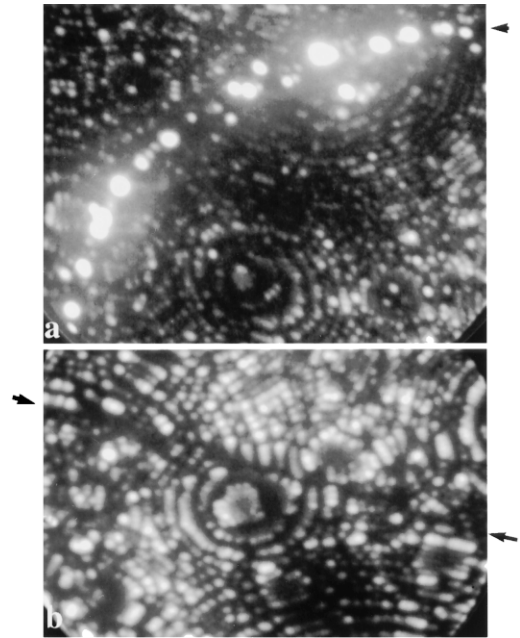


FIG. 2. Field ion micrographs of two different grain boundaries in boron-doped Ni₃Al demonstrating that the distribution of the brightly imaging atoms in the field ion micrographs, and hence, the boron coverage, varies significantly.

vealed that the distribution of the brightly imaging atoms in the field ion micrographs, and hence, the boron coverage, varies significantly. This variation was also observed along different regions of the same grain boundary as shown in Fig. 3. In some regions, the coverage was extremely low, for example, Figs. 3(a) and 3(d), whereas in other regions there was significantly higher coverage, for example, Fig. 3(c) and 3(e). Atom probe quantification of the boron level and the nickel to aluminum ratio at two grain boundaries is summarized in Table 1 [16]. In addition, the boron coverage along one of the grain boundaries was found to vary over a significant range of 9.4 to 61.9%. Similar wide variations were observed at other grain boundaries. The Ni:Al ratio was found to vary over a wide range, 2.2:1 to 3.4:1, in comparison to the Ni:Al ratio of close to 3.1 for the matrix in these Ni-24.2% Al materials. These studies were unable to find a simple correlation between the Ni:Al ratio and the boron coverage [16].

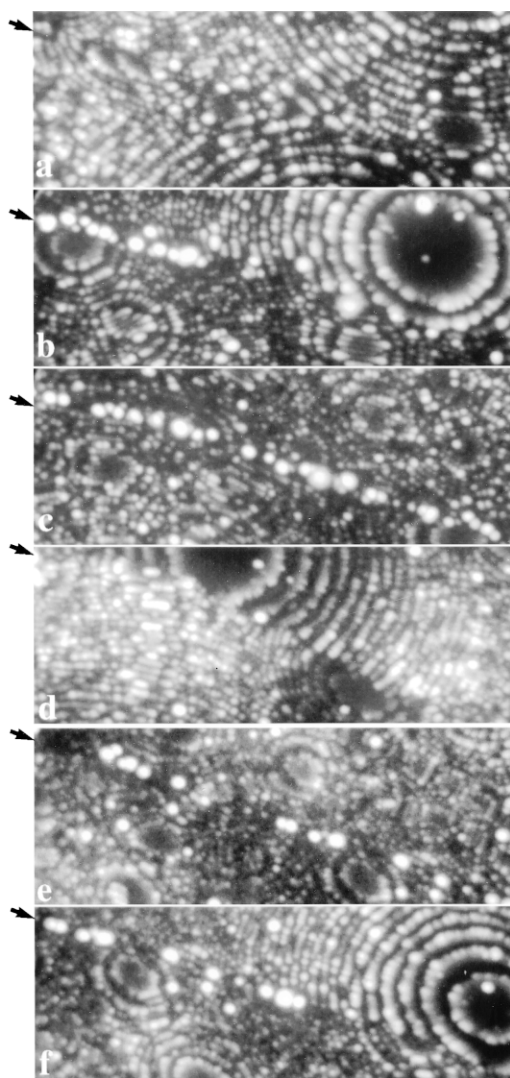


FIG. 3. Sequence of field ion micrographs of different regions of the same grain boundary in boron-doped Ni_3Al showing a variation in boron coverage along the grain boundary.

Sieloff et al. [17–22] also observed boron-decorated grain and antiphase boundaries in Ni_3Al alloys, and noted significant nickel enrichments and aluminum depletions in the vicinity of high-angle boundaries in Ni-enriched Ni_3Al alloys and variations in the boron coverage along the boundaries.

Some grain boundaries exhibited evidence of more spatially extensive boron segregation [10, 12–15]. In most of these cases, the boron segregation appeared as an

Table 1 The Gibbs Interfacial Excesses of Boron at Grain Boundaries in Ni_3Al

Analysis	Ni:Al ratio	Gibbs Interfacial Excess, Γ_i atoms m^{-2}	Coverage %
1a	3.40	4.5×10^{18}	26.7
1b	2.92	4.2×10^{18}	24.0
1c	2.23	4.8×10^{18}	27.0
1d	2.30	1.7×10^{18}	9.4
1e	2.81	3.6×10^{18}	20.4
1f	2.70	1.1×10^{19}	61.9
1 (avg.)	2.73	5.0×10^{18}	28.2
2 (avg.)	2.73	2.3×10^{18}	13.0

extended brightly imaging lenticular region at the grain boundary, as shown in Fig. 4. The maximum thickness of these regions was estimated to be $\sim 3\text{nm}$, their length was often larger than the field-of-view of the image, i.e., $> \sim 100\text{nm}$, and their composition was determined to be 26–31% Al and up to 5% B. It was suggested that this boron-enriched region was an ultrathin precipitate or grain boundary film rather than multilayer segregation [15]. However, the measured composition was too low to correspond to the τ phase (nickel–aluminum–boride). In addition to this extended morphology, some 5 to 10nm long boron-enriched regions were observed [9], as shown in Fig. 1(a). Most of the segments of the grain boundary shown exhibited low coverage with only an isolated boron atom evident. However, a small facet that exhibited significantly higher boron coverage was also observed. This observation indi-

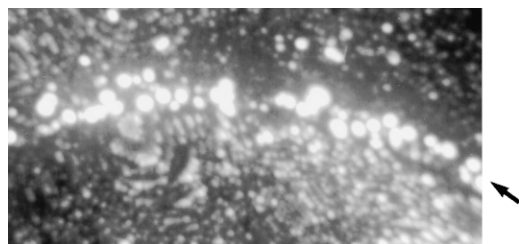


FIG. 4. An extended brightly imaging lenticular region $\sim 3\text{nm}$ thick at a grain boundary in boron-doped Ni_3Al .

cates that the local boundary plane can have a strong influence on the segregation behavior.

Atom probe field ion microscopy investigations also revealed that boron segregates to dislocations, low-angle boundaries, and stacking faults, as shown in Figs. 5, 6, and 7, respectively [13, 14]. In the cases of the low-angle boundary and the stacking fault, the boron decoration was more clearly revealed in field ion micrographs that were taken during field evaporation, shown in Figs. 6(b) and 7(b), because the contrast due to the individual atomic terraces (i.e., the concentric rings) is minimized rendering the brightly imaging boron atoms more prominent. It is evident from these field ion micrographs that the width of the segregation was narrow indicating that the boron segregation was confined to the interface plane. It was suggested that boron segregation to the dislocations, low-angle boundaries, stacking faults, and antiphase boundaries influences the mechanical properties through a solute drag-type mechanism [12, 16].

No ultrafine intragranular precipitates have been observed in these boron-doped Ni-24.2% Al alloys. However, boron clustering has been observed in alloys with higher aluminum contents (Ni-25% Al and Ni-26% Al), as shown in Fig. 8 [15]. These features were found to contain up to approximately 10 boron atoms and were clas-

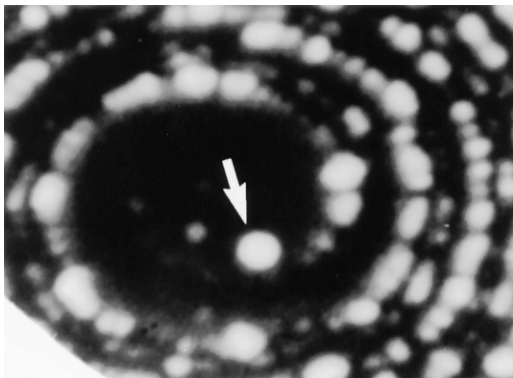


FIG. 5. Field ion micrograph of a boron-decorated dislocation in boron-doped Ni_3Al . The bright spot at the core of the dislocation is a boron atom.

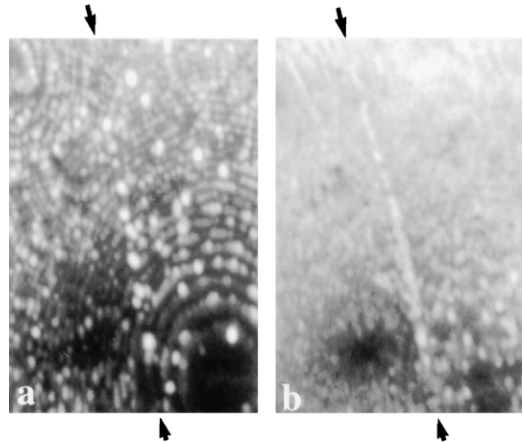


FIG. 6. (a) Field ion and (b) field evaporation micrographs of a boron-decorated low-angle boundary in boron-doped Ni_3Al .

sified as clusters due to their small size and the absence of any other elements.

BORON, CARBON, AND BERYLLIUM ADDITIONS TO NiAl

The solute distribution in B2-ordered NiAl has also been characterized with the atom probe [16, 23–31]. The matrix solubility of boron in NiAl was found to be distinctly different from that in boron-doped Ni_3Al . Atom probe analysis revealed that most of

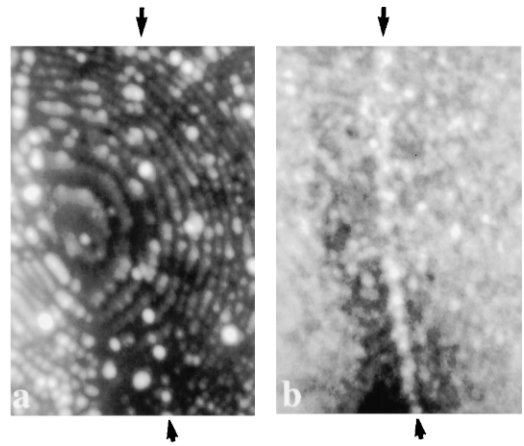


FIG. 7. (a) Field ion and (b) field evaporation micrographs of a boron-decorated stacking fault in cold-worked boron-doped Ni_3Al .

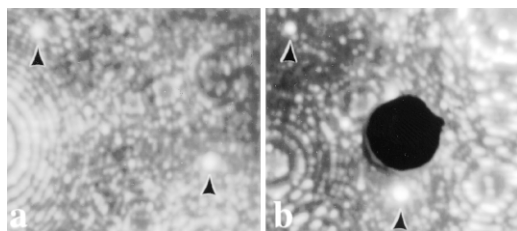


FIG. 8. Boron clusters in (a) boron-doped Ni-25% Al and (b) boron-doped Ni-26% Al alloys.

the boron addition remained in solid solution in the Ni_3Al . However, atom probe analysis of the matrix in an $\text{NiAl} + 0.15\%$ B alloy performed by Jayaram and Miller revealed that the boron solubility in NiAl was extremely low ($0.003 \pm 0.0007\%$ B after aging for 1 h at 500°C and $0.026 \pm 0.003\%$ B after aging for 1 h at 1100°C) [23]. Similar low matrix levels of $0.003 \pm 0.001\%$ C and $0.006 \pm 0.002\%$ C were measured by Jayaram and Miller in a carbon-doped (0.1% C) NiAl aged for 1 h at 500°C and 1 h at 1100°C , respectively [31]. In contrast, Jayaram and Miller found only small depletions in the beryllium content of the matrix in a $\text{NiAl} + 0.25\%$ Be alloy [23, 28].

The solute concentrations and boron coverages at grain boundaries have been characterized in binary and ternary NiAl alloys. Camus et al. [24, 25] demonstrated that approximately two-thirds of the analyzed grain boundaries in a binary Ni-49% Al alloy were depleted in aluminum to $\sim 40 \pm 1\%$ Al, and the remaining one-third did not exhibit any significant depletion. Boron was also found to segregate to the grain boundaries in boron-doped NiAl [23], as shown in Fig. 9. As in the case of Ni_3Al , the variation of the brightly imaging boron atoms indicated that the boron coverage varied along the grain boundary. The results of several analyses along this boundary are summarized in order in Table 2 [16]. The boron coverage was found to vary by a factor of ~ 7.5 from 3.6 to 27.4% ($\Gamma_i = 6.2$ to 46.3×10^{17} atoms m^{-2}). Most sections of the boundary exhibited nickel depletion (Ni:Al = 0.84), with one section exhibiting a significant nickel enrichment (Ni:Al = 1.27). Boron enrichment was observed in

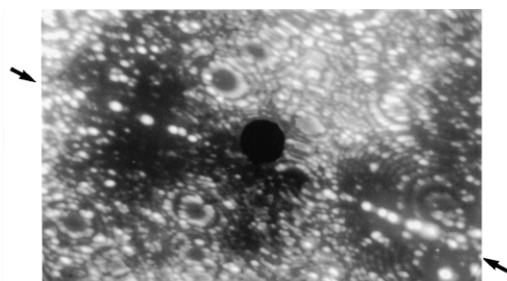


FIG. 9. Field ion micrograph of boron segregation to a grain boundary in boron-doped NiAl .

both nickel-depleted and nickel-enriched sections. No strong correlation between the Ni:Al ratio and the coverage was apparent in these data. In agreement with Auger studies, no evidence of carbon or beryllium segregation to grain boundaries was observed in carbon-doped or beryllium-doped NiAl [23, 28, 31].

The majority of the boron in boron-doped NiAl was determined by Jayaram and Miller to be in ultrafine precipitates ranging in size from 1 to 20nm [23], as shown in Fig. 10. Atom probe analysis revealed that the composition of the precipitate was consistent with that of an MB_2 type precipitate where the metallic content M was a mixture of titanium, vanadium, chro-

Table 2 The Gibbs Interfacial Excesses of Boron at a $\Sigma 3$ Coincident Site Lattice Grain Boundary in $\text{NiAl} + 0.04\%$ B Aged 1 h at 900°C

Analysis	Ni:Al ratio	Gibbs Interfacial Excess, Γ_i atoms m^{-2}	Coverage (%)
1	0.77	9.6×10^{17}	5.7
2	0.91	6.2×10^{17}	3.6
3	1.27	8.7×10^{17}	5.2
4	0.79	8.7×10^{17}	5.2
5	0.80	1.2×10^{18}	7.2
6	0.88	1.3×10^{18}	7.6
7	0.84	2.3×10^{18}	13.4
8	0.94	1.5×10^{18}	9.1
9	0.82	1.9×10^{18}	11.0
10	0.81	4.6×10^{18}	27.4
Average	0.88	1.6×10^{18}	9.5

mium, and tungsten. The metallic content was found to vary significantly from precipitate to precipitate, suggesting that these precipitates were formed from the trace elements in the material. Some carbon was also detected in these precipitates. Similar ultrafine MC precipitates have also been observed in carbon-doped NiAl [31] and in undoped single-crystal NiAl [24]. Due to their small size and relatively high number density, these precipitates produce significant precipitation hardening and are, therefore, detrimental to the mechanical properties. This precipitation hardening also offsets the benefits of the boron segregation to the high-angle grain boundaries. It has been shown that the number density of these precipitates can be decreased by reducing the quantities of trace impurities in the alloy by zone refinement [24]. Alternatively, the number density of these precipitates can be reduced and their size increased by an appropriate heat treatment [23].

ZIRCONIUM AND HAFNIUM SEGREGATION

Segregation of zirconium to dislocations in a NiAl alloy doped with 0.4% Zr has been directly observed by Jayaram and Miller [32, 33]. Approximately two-thirds of the $\langle 100 \rangle$ dislocations exhibited zirconium segregation after a heat treatment of 1 h at 1,000°C followed by a step-cooling sequence of 4 h at 800°C, 24 h at 600°C, 72 h at 400°C, as shown in Fig. 11. Zirconium-rich regions with ribbon-like morphologies 1 to 2 nm in width, a monolayer thick and 10 to

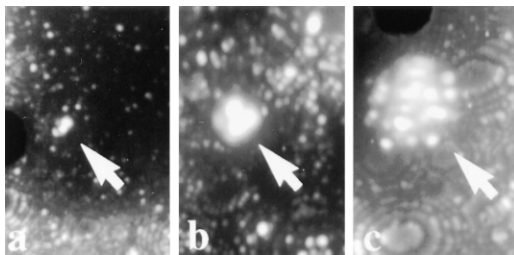


FIG. 10. Field ion micrographs of ultrafine (1 to 20nm) MB_2 precipitates in boron-doped NiAl.

25nm in length were also detected in the NiAl matrix, as shown in Fig. 12. It was suggested that these results indicated that the observed increase in the ductile-to-brittle temperature in these zirconium-based alloys was due to pinning of the dislocations by zirconium. Zirconium segregation of up to $\sim 60\%$ of a monolayer was measured at the grain boundaries. A boundary with relatively low zirconium coverage is shown in Fig. 13. The matrix was found to be heavily depleted in zirconium to a level of $0.007 \pm 0.002\%$ Zr.

Larson, Miller, and Noebe investigated the segregation of hafnium to dislocations in a single crystal Ni-51.4% Al-0.3% Hf alloy that was tested to compressive strains of $\sim 1-4\%$ in the [001] direction at 800K. The average hafnium content at the dislocations was found to be $0.44 \pm 0.18\%$, and was enriched by a factor of 2 over the experimentally determined matrix level of $0.22 \pm 0.02\%$ Hf. Brenner et al. reported hafnium segregation to grain boundaries in a cast Ni-23.5% Al-0.24% B-0.5% Hf alloy [17].

MOLYBDENUM ADDITIONS TO NiAl

The effect of molybdenum additions to NiAl have also been studied by Miller et al. [16, 34] to determine the cause of the large increase in the yield strength between the undoped material (154MPa) and the molybdenum-doped alloy (254MPa). Extensive characterization was performed of a grain boundary in NiAl containing 0.7% Mo annealed for 1 h at 1,000°C and 1 h at

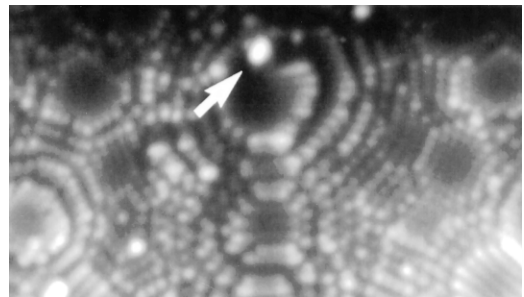


FIG. 11. Field ion micrograph of a zirconium decorated dislocation in NiAl doped with 0.4% Zr.

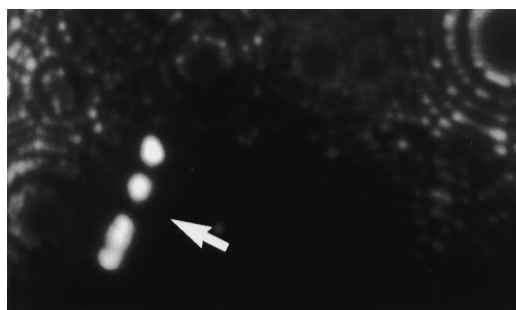


FIG. 12. Field ion micrograph of a zirconium-rich region with a ribbon-like morphology 1 to 2nm wide, a monolayer thick and 10 to 25nm in length in zirconium-doped NiAl.

500°C. A field ion micrograph of this $\Sigma 3$ coincident site lattice boundary is shown in Fig. 14. A 2-1/2 D reconstruction [34] of the solute distribution measured in an atom probe analysis along the plane of the boundary is shown in Fig. 15. Although most of the solute was distributed uniformly along the grain boundary, there was some visual evidence of regions of higher than average local concentrations of iron, molybdenum, nitrogen, and carbon, and also some evidence of molybdenum–nitrogen coenrichment. This small nonuniformity in the solute distribution may arise from small changes in the boundary plane or the presence of grain boundary dislocations that changes the local atomic environment and thereby influences the segregation behavior. The Gibbsian interfacial

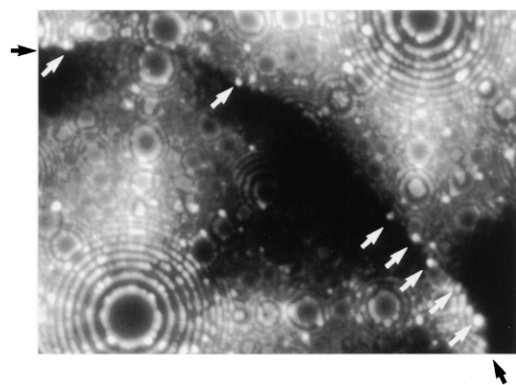


FIG. 13. Field ion micrograph of a zirconium-decorated grain boundary in NiAl doped with 0.4% Zr

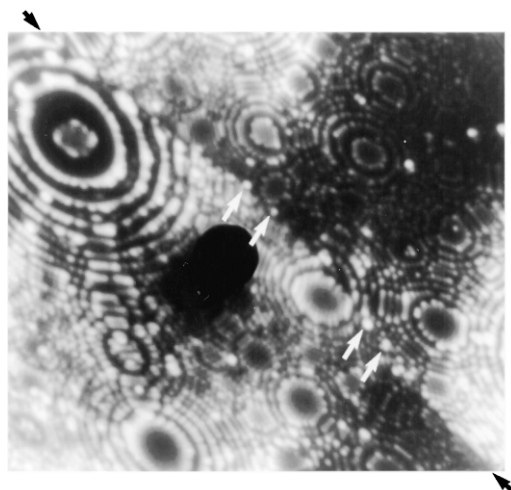


FIG. 14. Field ion micrograph of a $\Sigma 3$ coincident site lattice boundary in NiAl containing 0.7% Mo annealed for 1 h at 1,000°C and 1 h at 500°C.

excesses of all the detected solutes along this boundary are summarized in Table 3. Small but significant enrichments of molybdenum, nitrogen and silicon, carbon, boron, and iron are evident at the grain boundary.

Atom probe analysis indicated extremely low solubilities of the molybdenum and other trace impurities in the matrix of the molybdenum-doped NiAl [34]. The average composition of the matrix was measured to be Ni-50.4 \pm 1.2% Al-0.005 \pm 0.001% Mo with 0.007 \pm 0.002% Fe, 0.005 \pm 0.001% Si and N, and 0.0004 \pm 0.0004% V. The large error on the aluminum content indicates a significant inhomogeneity from one region to another.

The majority of the molybdenum was found to be concentrated in a low number density (~ 1 to $2 \times 10^{21} \text{ m}^{-3}$) of 10 to 50nm diameter spherical molybdenum precipitates [34]. These body-centered cubic precipitates were observed both in the NiAl matrix, as shown in Fig. 16, and also at grain boundaries. Their composition was determined to be Mo-3.3 \pm 0.6% Al, with residual amounts of 0.06 \pm 0.03% B, 0.04 \pm 0.02% Ni, 0.01 \pm 0.01% Fe, and 0.04 \pm 0.02% V. Calculations based on an Orowan mechanism indicate that these precipitates

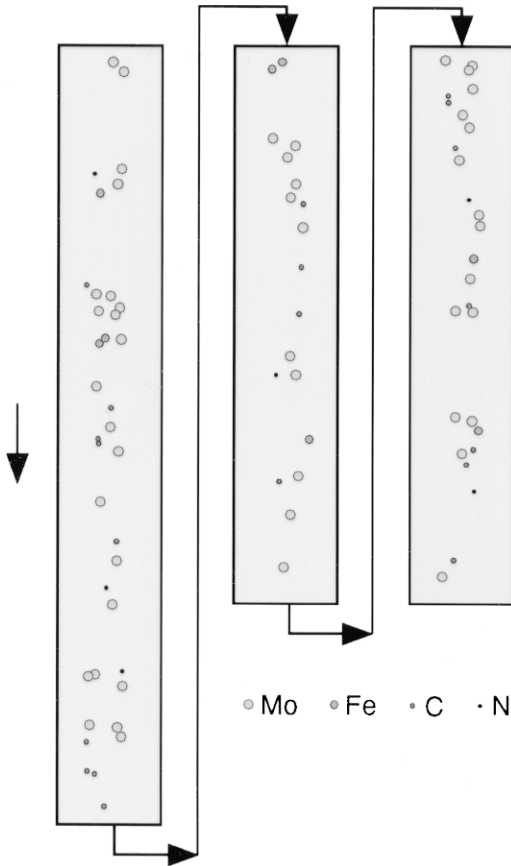


FIG. 15. A 2-1/2 D reconstruction of the solute distribution measured in an atom probe analysis along the plane of the grain boundary shown in Fig. 14. Each symbol is an individual solute atom. The nickel and aluminum atoms are not shown.

generate a significant increase in yield stress of between 82 and 210MPa, depending on the measured minimum and maximum size of the precipitate. These values were found to be in good agreement with the differences in the yield stresses of the molybdenum-doped and undoped alloys (100MPa), because a larger number of the smaller diameter precipitates were observed, which would indicate that the value at the lower end of this calculated range is more appropriate.

SITE OCCUPATION STUDIES IN NICKEL ALUMINIDES

By measuring the composition of individual planes of atoms in the atom probe, the

Table 3 The Gibbs Interfacial Excesses of Solute at a $\Sigma 3$ Coincident Site Lattice Grain Boundary in NiAl + 0.7% Mo Aged 1 h at 1,000°C and 1 h at 500°C

Element	Gibbs interfacial excess, Γ_i atoms m^{-2}	Coverage %
Mo	9.9×10^{16}	0.58
N/Si	6.5×10^{16}	0.38
C	1.1×10^{16}	0.07
B	5.7×10^{15}	0.03
Fe	3.8×10^{15}	0.02

site occupancy of solutes can be determined [1, 2, 35]. The site occupancy of substitutional solutes has been studied by Miller et al. [36, 37] in Ni₃Al alloys containing hafnium, cobalt, and iron additions. These studies revealed that hafnium has a strong preference and iron has a weak preference for the aluminum sites, whereas cobalt has a preference for the nickel sites. A comparison of atom probe results with those determined by atom location by channeling electron microanalysis (ALCHEMI) showed similar site preferences [37]. Hono et al. [38–40] have characterized the site occupancy of copper and germanium in Ni₃Al. The copper was found to prefer the nickel sites. In the germanium-containing alloy, the behavior was found to depend on the stoichi-

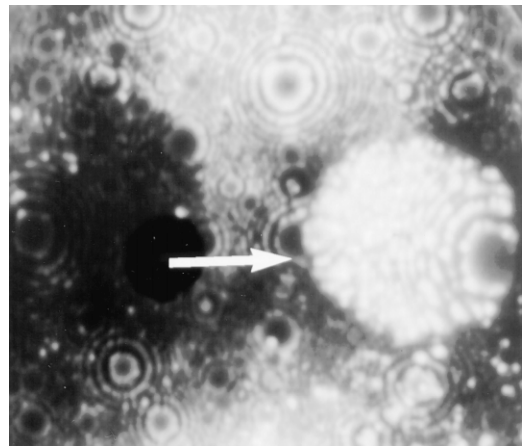


FIG. 16. Field ion micrograph of brightly imaging 10- to 50-nm diameter spherical molybdenum precipitates in NiAl containing 0.7% Mo.

ometry of the alloy. In aluminum-rich alloys, the germanium was approximately equally distributed between the nickel and aluminum sites, whereas, as the aluminum content of the alloy was decreased, the germanium preferred the aluminum sites.

TITANIUM ALUMINIDES

Two-phase $\alpha_2+\gamma$ TiAl alloys are attractive for structural applications at elevated temperatures because they possess good high-temperature mechanical properties, low density, and good creep and oxidation resistance. However, extensive use of these alloys has been limited by their low ductility and poor fracture resistance at ambient temperatures. Efforts to enhance ductility and improve other mechanical properties have focused on microstructural control with a variety of microalloying additions including B, Cr, Mn, Mo, Nb, Si, V, and W. In addition, investigations of $\alpha_2+\gamma$ TiAl alloys containing additional phases, such as the β phase, have found good mechanical properties.

INITIAL INVESTIGATIONS AND MICROSTRUCTURAL OBSERVATIONS

The Ti_3Al α_2 phase (D0_{19} -ordered structure) is stronger, but also denser, than the near equiatomic TiAl γ phase (L1_0 -ordered structure). Three common types of microstructure in two-phase $\alpha_2+\gamma$ TiAl alloys are equiaxed γ , duplex, and lamellar structures. The lamellar microstructure usually consists of thin plates of the γ and the α_2 phases oriented with $(0001)_{\alpha_2} \parallel (111)_{\gamma}$, and $\langle 1120 \rangle_{\alpha_2} \parallel \langle 110 \rangle_{\gamma}$. Transmission electron and field ion micrographs of a TiAl-based alloy with a lamellar structure are shown in Fig. 17.

The first atom probe investigation of a titanium aluminide alloy was performed by Menand et al. in 1986 [41] on binary Ti-54% Al. A very small volume fraction of α_2 phase was present and was determined to be rich in titanium ($\sim\text{Ti}_2\text{Al}$). The material was brittle and difficult to analyze. Two

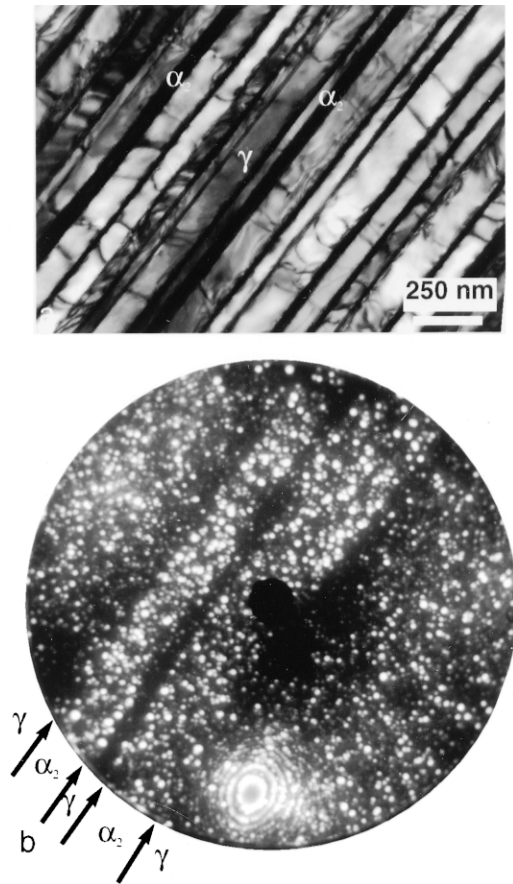


FIG. 17. (a) Transmission electron and (b) field ion micrographs of the lamellar TiAl microstructure in the stress-relieved Ti-47% Al-2% Cr-1.8% Nb-0.15% B-0.20% W alloy.

years later, a manganese-modified alloy (as-cast and aged 24 h at $1,000^\circ\text{C}$) was investigated by Hanamura et al. [42] and later by Saga et al. [43], as methods of improving ductility were sought in the γ -based materials. The addition of manganese was determined to stabilize twin structures against dissolution during annealing.

Liu et al. [44–47] performed the first detailed microstructural investigations of a binary Ti-48% Al alloy and a Ti-46% Al-1% Cr-0.2% Si alloy with a grain size of 100–200 μm , and a lamellar spacing of 0.2–2 μm . High-quality field ion images of the α_2 and γ phases were observed and ordered-pole analyses indicated titanium-antistructure atoms present in the aluminum layers

[44]. A high degree of ordering was determined for both alloys and the addition of chromium was observed to promote thermally formed antiphase boundaries [45, 46]. The addition of chromium and silicon was observed to raise the aluminum level in the α_2 phase and to promote thinner lamellae in the microstructure [46]. Interfaces between γ plates were observed in "true twin" and "pseudotwin" orientations on the (111) plane with a ~ 7 nm-thick region of the α_2 phase present between the γ plates in the pseudotwin orientation [46]. Investigation of (011) twinning in a Ti-45% Al-5% V alloy was also conducted by Liu et al. [47].

INTERSTITIAL SOLUBILITY AND PARTITIONING

In an effort to elucidate the mechanism responsible for ductility enhancement in $\alpha_2 + \gamma$ alloys compared to single-phase TiAl alloys, Uemori et al. [48] investigated the oxygen behavior in an oxygen-doped Ti-50% Al alloy annealed for 24 h at 1,000°C. Qualitative results of significant oxygen enhancement in the α_2 phase were found [48]. This result was later quantitatively confirmed by Denquin et al. [49] in cast Ti-46% Al and Ti-48% Al alloys containing nominal oxygen levels of less than 0.30% O. Oxygen concentrations in the α_2 phase of the 46% Al and 48% Al alloys were determined to be $0.81 \pm 0.07\%$ and $1.92 \pm 0.12\%$, respectively. These results appeared to support the theory that the presence of the α_2 phase in two-phase alloys improves ductility by scavenging interstitial impurities, thus lowering the oxygen content in the γ phase and changing the deformation mechanism [50, 51]. A three-dimensional atom probe analysis of oxygen partitioning to the α_2 phase is shown in Fig. 18.

However, the results of Denquin et al. [49] also showed almost equal oxygen levels in the γ phase of the 46% Al ($0.020 \pm 0.01\%$ O) and 48% Al ($0.023 \pm 0.007\%$ O) alloys despite a large difference in α_2 phase volume fraction between the two alloys (~ 30 and $\sim 10\%$, respectively). This suggests that the maximum solubility of oxy-

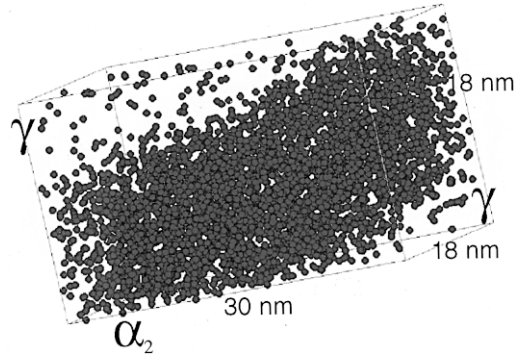


FIG. 18. A three-dimensional atom map showing the oxygen distribution between the γ and α_2 phases in the stress-relieved Ti-47% Al-2% Cr-1.8% Nb-0.15% B-0.20% W alloy.

gen in the γ phase is very near these low values. This was verified by Menand et al. [52, 53] in further work on single-phase γ and two-phase alloys, which quantified the oxygen solubility in the γ phase at $\sim 0.025\%$. Thus, the improved ductility in $\alpha_2 + \gamma$ alloys cannot be completely explained by impurity scavenging by the α_2 phase lowering the oxygen content in the γ phase. Further evidence of the lack of correlation between the γ phase oxygen solubility and mechanical properties was provided by Menand et al. [53, 54] in a study of single-phase γ alloys doped with Cr, Mn, or Nb. In view of the lack of variation in the γ phase oxygen levels when ternary additions known to modify strength and oxidation resistance were added, it was proposed that oxygen *in solution* does not play a major role in the mechanical properties of γ -based TiAl alloys [54].

The behavior of carbon and nitrogen in single-phase γ and two-phase alloys has also been investigated. Carbon is preferentially located in the α_2 phase, although the partitioning is not as strong as for oxygen. In a cast two-phase Ti-48% Al alloy having an overall carbon content of $0.056 \pm 0.003\%$, the carbon levels in the γ and α_2 phases were determined to be 0.033 ± 0.007 and $0.106 \pm 0.04\%$, respectively [53]. In single-phase γ Ti-52% Al having an overall carbon content of $0.034 \pm 0.002\%$, the carbon level was determined to be $0.012 \pm 0.008\%$ [52].

Quantitative analysis of nitrogen is difficult in the atom probe due to the direct overlap in mass-to-charge state ratios of singly charged nitrogen and doubly charged aluminum hydride species. Like oxygen and carbon, however, nitrogen appears to be preferentially located in the α_2 phase [52, 53].

TERNARY ELEMENT PARTITIONING

To understand the effect of alloying elements on mechanical behavior, it is beneficial to know how various elements distribute themselves between the phases present. The partitioning behavior of chromium, niobium, and tungsten has been studied by Larson et al. [55–58] in a Ti-47% Al-2% Cr-1.8% Nb-0.15% B-0.20% W alloy that was cast and extruded at a temperature above T_α ($\sim 1,320^\circ\text{C}$). In material that was stress relieved for 2 h at 900°C , atom probe results show that the tungsten is enriched in the α_2 phase with a partitioning factor of $\sim 2:1$. Chromium was also found to partition preferentially to the α_2 phase with a partitioning factor of $\sim 1.8:1$. This trend is in agreement with previous results from Inui et al. [59] for nonannealed samples. The niobium exhibited a lower partitioning factor with only a slight preference for the γ phase. A standard lever rule calculation yields α_2 volume fractions after this heat treatment of 32, 23, and 24% using the experimental concentrations of chromium, niobium, and tungsten, respectively. Note that these values are higher than expected, but the material has probably not yet attained equilibrium volume fractions.

In the same alloy aged 720 h at 800°C , the tungsten partitioning behavior has reversed and the average tungsten in the γ phase was above the nominal alloy level [58]. Aging also resulted in a redistribution of the chromium to approximately equal values in each phase, but did not affect the niobium levels significantly. To investigate whether the partitioning behavior in the stress relieved state is representative of the $\alpha+\gamma$ region, as opposed to $\alpha_2+\gamma$, Larson et al. [60] have investigated partitioning in material (aged 2,184 h at 800°C) that was re-

heated into the $\alpha+\gamma$ phase field for 2 h at 1210°C and water quenched. After this heat treatment, the partitioning to the α_2 phase of chromium, and to a lesser extent tungsten, is similar to that measured after 2 h at 900°C . This suggests that the 2 h at 900°C measurement is also representative of phase compositions from the higher temperature α/γ region. (It should be noted that macrosegregation is likely to occur in this alloy, which may affect the calculated partitioning factors for the alloying elements.)

The partitioning of chromium and niobium has also been studied by Menand et al. [61] in a Ti-48% Al-2% Cr-2% Nb alloy that was heat treated for 1 h at 1420°C and furnace cooled. Atom probe results show that the α_2 phase is enriched in chromium (partitioning factor of $\sim 2.6:1$), and the γ phase is enriched in niobium (partitioning factor of $\sim 2.3:1$). In an alloy of the same composition that was oil quenched and annealed for 96 h at $1,000^\circ\text{C}$, the chromium was distributed approximately equally between the α_2 and γ phases, whereas the niobium remained partitioned to the γ phase [61]. Further evidence of chromium partitioning to the α_2 phase in a two-phase Ti-48% Al-2% Cr alloy that was heat treated for 5 h at 900°C and furnace cooled has been shown by Kim et al. [62].

The partitioning behavior of various elements in a tantalum-modified alloy has been investigated by Larson et al. [63] in Ti-47% Al-2% Cr-1% Nb-0.15% B-0.2% W-0.8% Ta, which was rapidly solidified. In material that was stress relieved for 2 h at 900°C , atom probe results indicate that the tungsten is enriched in the α_2 phase with a partitioning factor of $\sim 1.5:1$, and this increases slightly with aging (2,160 h at 800°C). In the stress-relieved alloy, the chromium was found to partition only slightly to the α_2 phase with a partitioning factor of $\sim 1.2:1$. This partitioning increased upon aging, although this seems to be primarily the result of a lower concentration in the γ phase. The niobium did not exhibit a significant preference for either α_2 or γ phase in the stress-relieved or aged alloys. No statistically significant tantalum partitioning in

either the stress-relieved or aged alloys was observed despite a previous compositional measurement of tantalum in an $\alpha_2 + \gamma$ TiAl alloy suggesting slight partitioning to the α_2 phase [64].

SITE OCCUPATION STUDIES IN TITANIUM ALUMINIDES

As noted above, numerous alloying elements have been added to TiAl alloys in attempts to improve mechanical properties, ductility, oxidation resistance, etc. Site-occupation studies for niobium have been performed on single-phase γ Ti-54% Al-5% Nb and two-phase Ti-45% Al-5% Nb. In the γ phase of both alloys, niobium was found exclusively in the titanium layers [65]. Similarly, in the γ phase of a two-phase Ti-45% Al-5% V alloy, vanadium was preferentially located on the titanium sublattice [65].

The site-occupation probability of chromium has also been investigated with the use of atom probe analysis. Results reported by Wesemann et al. [66] suggest that chromium has a strong preference for occupying titanium sites in the γ phase of a two-phase Ti-46% Al-3% Cr alloy. These results appear to be questionable, however, in view of results obtained with the AL-CHEMI technique, which show a majority of the chromium atoms to be located on aluminum sites [67].

In efforts to improve the oxidation and corrosion resistance of TiAl alloys, the effects of ruthenium additions have been investigated in the γ phase of a two-phase Ti-48% Al-2% Ru alloy [68]. The results show a high probability for ruthenium to occupy aluminum sites, and are supported by results from X-ray analysis.

BORON DOPING

One alloying element that results in large modifications to TiAl alloys is boron. Because the atom probe is equally sensitive to all elements, it provides a means to investigate the behavior of light elements, such as boron, which cannot be easily examined using transmission electron microscopy with traditional energy dispersive X-ray spec-

troscopy. Boron additions in TiAl alloys result in refinements in grain size [69] and lamellar spacing [70], as well as a modification of the strain hardening behavior [71].

Atom probe research quantifying boron solubilities in TiAl alloys has been reported by Larson et al. [72] in a Ti-47% Al-2% Cr-1.8% Nb-0.15% B-0.20% W alloy. The boron concentrations were found to be significantly depleted below the nominal alloy concentration in both α_2 and γ phases in a stress-relieved and an aged state [58]. The boron solubilities after annealing 720 h at 800°C are estimated to be 0.032 ± 0.015 and $0.028 \pm 0.018\%$, in the γ and α_2 phases, respectively. These levels are of the order of those determined by Menand et al. [49, 52, 53, 61] for oxygen solubility in the γ phase, but boron does not appear to partition to the α_2 phase, as has been observed for other interstitial elements. The majority of the boron was in a variety of borides, including TiB, TiB₂, and (Ti,Cr)₂B. A field ion micrograph of a (Ti,Cr)₂B precipitate is shown in Fig. 19. The MB₂ phase, which was prevalent in this alloy, is metal enriched for the borides detected, containing ~37 and ~41% M in the stress-relieved and aged alloys, respectively. The metallic portion of the MB₂ phase is primarily titanium, but a significant amount of the alloying additions are contained in the chromium-enriched M₂B phase. A summary of boride compositions analyzed in both the stress-relieved and aged states of Ti-47% Al-2% Cr-1.8% Nb-0.15% B-0.20% W is shown in Table 4 [58].

Microstructural characterization of boron in a rapidly solidified Ti-47% Al-2% Cr-1% Nb-0.15% B-0.2% W-0.8% Ta alloy has also been investigated by Larson et al. [63]. Boron solubilities after long-term annealing in this alloy are estimated to be 0.012 ± 0.007 and $0.04 \pm 0.04\%$, in the γ and α_2 phases, respectively. The (Ti,Ta)B and (Ti,Cr,Ta)₂B phases were detected in this alloy. The MB phase is metal enriched for the borides detected, containing ~54% M in an alloy heat treated for 2 h at 900°C. The metallic portion of the MB phase is primarily Ti (~73%) and Ta (~17%) with small amounts of W and Nb.

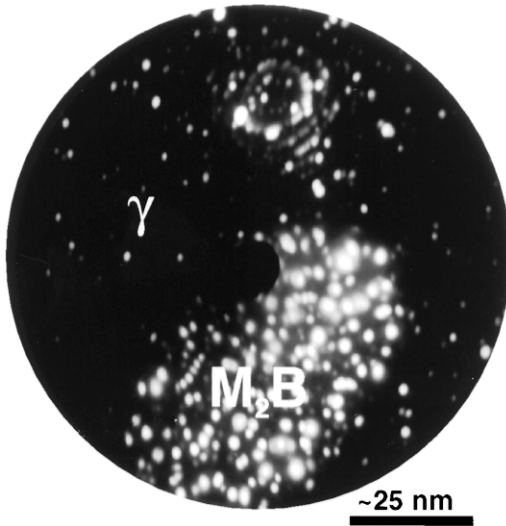


FIG. 19. Field ion micrograph showing a (Ti,Cr)₂B precipitate in the stress-relieved Ti-47% Al-2% Cr-1.8% Nb-0.15% B-0.20% W alloy.

SEGREGATION STUDIES

Interphase interfaces in TiAl alloys have been investigated by Hanamura et al. [42] and by Saga et al. [43] in Ti-50% Al doped with 2 wt. % Mn. Qualitative evidence of manganese segregation to γ/γ interfaces [42] and α_2/γ interfaces [43] has been presented and it was suggested that the ductility was improved by manganese segregation promoting twin deformation due to increased twin dislocation stability. However, quantitative results of manganese segregation were minimal and the amount of manganese present in the matrix phases was not estimated.

More recently, atom probe studies of segregation in TiAl alloys have been performed by Larson et al. [55–58, 74] and by Menand et al. [61]. Larson et al. studied tungsten segregation in a Ti-47% Al-2% Cr-1.8% Nb-0.15% B-0.20% W alloy that was cast and extruded at a temperature above T_α (~1320°C). In material that was stress relieved for 2 h at 900°C, results showed significant tungsten segregation (1–5% W coverage) at both the γ/γ and α_2/γ interfaces [57, 73]. A field ion micrograph showing tungsten segregation (bright spots) at an α_2/γ interface is shown in Fig. 20. The behavior of tungsten alloying additions in this material is of particular interest because previous studies have shown that tungsten significantly reduced lamellar coarsening [70]. Chromium segregation to γ/γ interfaces was also reported [57], although no significant segregation of boron or niobium was found. A three-dimensional atom probe analysis of the partitioning and segregation behavior in the stress-relieved Ti-47% Al-2% Cr-1.8% Nb-0.15% B-0.20% W alloy is shown in Fig. 21. Compositions from six boundary regions in this alloy are given in Table 5. In Ti-47% Al-2% Cr-1.8% Nb-0.15% B-0.20% W, which was annealed for 720 h at 800°C, the amount of chromium and tungsten segregation was reduced [58]. However, Menand et al. reported chromium segregation at both γ/γ and α_2/γ interfaces in a Ti-48% Al-2% Cr-2% Nb alloy, which was homogenized for 1 h at 1,420°C and annealed for 96 h at 1,000°C [61].

Table 4 Boride Compositions in Ti-47% Al-2% Cr-1.8% Nb-0.15% B-0.20% W

Heat treatment	Measured composition	Phase
2 h at 900°C	(Ti _{94.3} Nb _{3.2} Cr _{1.1} W _{1.1} Al _{1.0}) B _{1.7}	MB ₂
2 h at 900°C	(Ti _{92.6} Nb _{2.5} Cr _{0.6} W _{0.6} Al _{1.4}) B _{1.05}	MB
2 h at 900°C	(Ti _{59.5} Nb _{9.5} Cr _{23.0} W _{5.3} Al _{2.7}) 2.06B	M ₂ B
720 h at 800°C	(Ti _{88.3} Nb _{2.5} Cr _{2.0} W _{3.1} Al _{4.1}) B _{1.4}	MB ₂
720 h at 800°C	(Ti _{95.8} Nb _{0.9} Cr ₀ W _{2.5} Al _{0.8}) B _{1.09}	MB
720 h at 800°C	(Ti _{64.2} Nb _{5.8} Cr _{14.5} W _{6.3} Al _{9.2}) 2.03B	M ₂ B

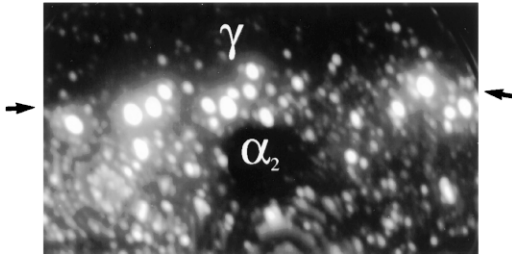


FIG. 20. Field ion micrograph showing tungsten (bright spots) segregated to an α_2/γ interface in the stress-relieved Ti-47% Al-2% Cr-1.8% Nb-0.15% B-0.20% W alloy.

POLYSYNTHETICALLY TWINNED TiAl

Polysynthetically twinned (PST) TiAl crystals have been developed to study the lamellar microstructure in two-phase TiAl alloys [74]. PST TiAl materials contain no grain boundaries, and have a single set of aligned lamellae of α_2 and γ phases. Therefore, PST samples facilitate the study of the dependence of mechanical properties on lamellar structure by providing a known, consistent alignment of lamellae. Previous studies have shown that chromium and molybdenum segregation occurs at certain noncoherent γ/γ twin boundaries in PST TiAl. These studies also found a depletion of Al at certain γ/γ interfaces, showing “ α_2 -like” compositions [59]. The feasibility of applying atom probe field ion microscopy to PST TiAl samples has been examined, and some preliminary findings in both binary and zirconium-doped PST TiAl have been reported [75, 76].

OTHER TiAl-BASED STUDIES

Hono et al. [77] have performed atom probe investigations on small, untransformed regions in a massively transformed Ti-48% Al alloy to determine compositional variations in ultrafine α_2 and γ lamellae (5–10nm spacing). Significant differences in composition between the α_2 and γ phases indicated that portions of the microstructure did not evolve by a displacive or martensitic type transformation, as had been previously suggested.

The mechanism of α_2 phase formation in $\alpha + \alpha_2$ alloys has been investigated by Wood et al. [78] in a Ti-14.5% Al alloy. Preliminary results indicate that ordered regions of α_2 form in the alloy before significant composition variations are present, in agreement with atomistic simulations of phase separation using a dynamic Ising model [78]. Further work on this material, using atom probe analysis in conjunction with transmission electron microscopy and neutron diffraction [79], supports decomposition occurring via a conditional spinodal mechanism.

The effects of in situ microtwinning of TiAl in the field ion microscope has been examined by Larson et al. [80]. The field-induced stresses present under normal field ion imaging conditions were found to be sufficient to induce the formation of twin-oriented regions in the γ phase of Ti-47% Al-2% Cr-1.8% Nb-0.15% B-0.20% W, and Ti-47% Al-2% Cr-1% Nb-0.15% B-0.2% W-0.8% Ta [63, 80]. These regions can be very narrow in width (<5nm), and often resemble the α_2 phase in their field ion im-

Table 5 Compositions From Boundary Regions in Stress-Relieved Ti-47% Al-2% Cr-1.8% Nb-0.15% B-0.20% W

Region	Ti	Al	Cr	Nb	O	B	W
γ/γ	49.1 ± 1.0	46.2 ± 1.0	2.6 ± 0.32	1.7 ± 0.26	0.06 ± 0.05	0.04 ± 0.04	0.38 ± 0.13
γ/γ	44.2 ± 1.28	52 ± 1.29	1.53 ± 0.32	1.98 ± 0.36	0.02 ± 0.03	0.02 ± 0.03	0.33 ± 0.15
γ/γ	48.1 ± 0.87	47.6 ± 0.87	1.7 ± 0.23	2.2 ± 0.26	0.08 ± 0.05	0.02 ± 0.02	0.33 ± 0.10
α_2/γ	60.5 ± 2.7	33 ± 2.6	2.73 ± 0.90	2.04 ± 0.78	1.06 ± 0.56	—	0.68 ± 0.45
α_2/γ	54.6 ± 1.9	39.8 ± 1.9	1.95 ± 0.54	2.14 ± 0.57	0.92 ± 0.37	0.15 ± 0.15	0.42 ± 0.25
α_2/γ	58.3 ± 2.2	34.6 ± 2.1	3.73 ± 0.85	1.40 ± 0.53	1.29 ± 0.50	0.06 ± 0.11	0.42 ± 0.29

Error bars are given as $\pm 2\sigma$.

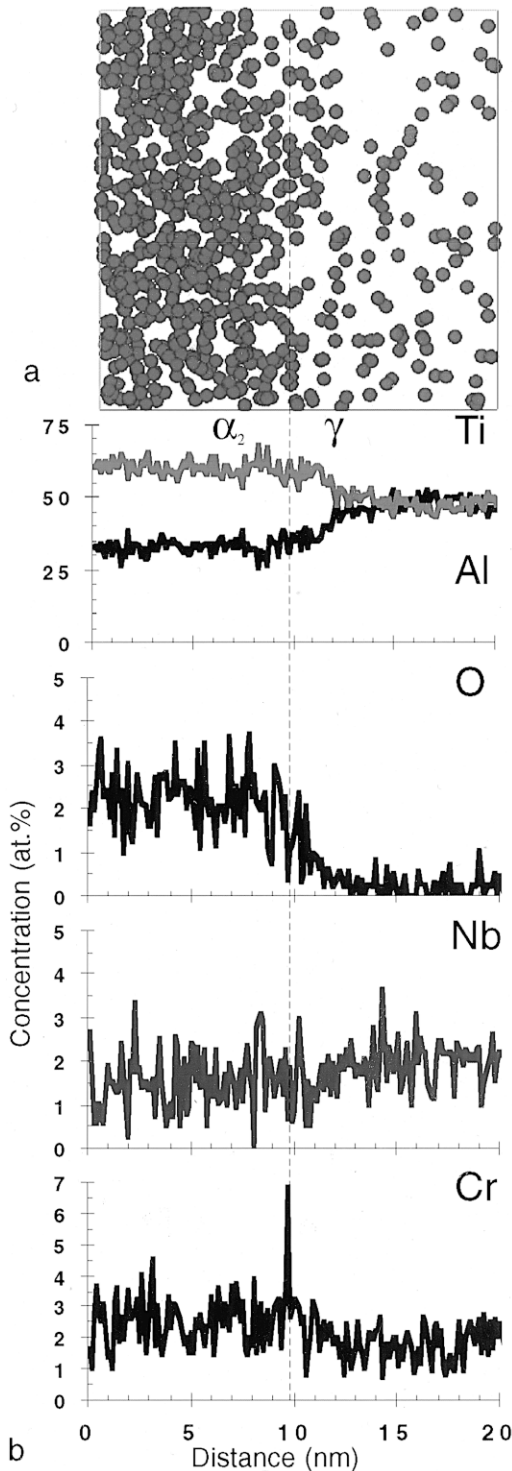


FIG. 21. Three-dimensional atom probe analysis showing (a) oxygen distribution in the γ and α_2 phases, and (b) composition profiles across the α_2/γ interface showing partitioning and/or segregation behavior of Ti, Al, O, Nb, and Cr.

aging characteristics. Larson et al. [81] have also performed a survey of the field ion imaging behavior of several different TiAl-based alloys, including two-phase alloys, single-phase α_2 , and single-phase γ microstructures.

The authors would like to thank K. F. Russell for her technical assistance, Prof. M. L. Weaver for manuscript review, Drs. J. A. Horton, C. T. Liu, I. M. Anderson, A. J. Duncan, and R. Jayaram for their contributions to the results presented in this paper, and Dr. C. T. Liu and Prof. M. Yamaguchi for provision of material. This research was sponsored by the Division of Materials Sciences, U.S. Department of Energy, under Contract DE-AC05-96OR22464 with Lockheed Martin Energy Research Corp. This research was conducted utilizing the Shared Research Equipment User Program facilities at ORNL.

References

1. M. K. Miller and G. D. W. Smith: *Atom Probe Microanalysis: Principles and Applications to Materials Problems*, Materials Research Society, Pittsburgh, PA (1989).
2. M. K. Miller, A. Cerezo, M. G. Hetherington, and G. D. W. Smith: *Atom Probe Field Ion Microscopy*, Oxford University Press, Oxford, UK (1996).
3. C. T. Liu, J. Stringer, J. N. Mundy, L. L. Horton, and P. Angelini: Ordered intermetallic alloys: An assessment. *Intermetallics* 5:579–596 (1997).
4. K. Aoki and O. Izumi: Improvement in room temperature ductility of the LI_2 type intermetallic compound Ni_3Al by boron addition. *Nippon Kinzoku Gakkaishi* 43:1190–1196 (1979).
5. C. T. Liu, C. L. White, and J. A. Horton: Effect of boron on grain boundaries in Ni_3Al . *Acta Metall.* 33:213–229 (1985).
6. R. D. Noebe, R. R. Bowman, and M. V. Nathal: Physical and mechanical properties of the B2 compound $NiAl$. *Int. Mater. Rev.* 38:193–232 (1993).
7. C. T. Liu and J. A. Horton: Effect of refractory alloying additions on mechanical properties of near-stoichiometric $NiAl$. *Mater. Sci. Eng. A* 192/193: 170–178 (1995).
8. R. R. Bowman, R. D. Noebe, S. V. Raj, and I. E. Locci: Correlation of deformation mechanisms with the tensile and compressive behavior of $NiAl$ and $NiAl(Zr)$ intermetallic alloys. *Metall. Trans.* 23A:1493–1508 (1992).
9. M. K. Miller and J. A. Horton: An atom probe field ion microscope study of boron decorated grain

- boundaries in Ni₃Al. *Scripta Metall.* 20:789–792 (1986).
10. J. A. Horton and M. K. Miller: A TEM-APFIM investigation of boron-doped Ni₃Al. *J. Phys.* 47-C2: 209–214 (1986).
 11. M. K. Miller and J. A. Horton: Boron distribution at boundaries in rapidly-solidified Ni₃Al. *J. Phys.* 47-C7:263–268 (1986).
 12. J. A. Horton and M. K. Miller: Atom probe analysis of grain boundaries in rapidly-solidified Ni₃Al. *Acta Metall.* 35:133–141 (1987).
 13. J. A. Horton and M. K. Miller: *An Atom Probe Study of Boron Segregation to Line and Planar Defects in Ni₃Al*. Proc. High Temperature Ordered Intermetallic Alloys II, N. S. Stoloff, C. C. Koch, C. T. Liu, and O. Izumi, eds., Boston, MA (December 2–4, 1987) Materials Research Society, Pittsburgh, PA, 81:105–110 (1987).
 14. M. K. Miller and J. A. Horton: Direct observation of boron segregation to line and planar defects in Ni₃Al. *J. Phys.* 48-C6:379–384 (1987).
 15. J. A. Horton, M. K. Miller, C. T. Liu, E. P. George, and J. Bentley: *Effect of Aluminum Level on Boron Clustering in Ni₃Al*. Proc. High Temperature Ordered Intermetallic Alloys III, C. T. Liu, A. I. Taub, N. S. Stoloff, and C. C. Koch, eds., Boston, MA (November 29–December 1, 1988) Materials Research Society, Pittsburgh, PA, 133:89–97 (1989).
 16. M. K. Miller: *Atomic Level Microstructural Characterization by APFIM*. Proc. Microstructures and Functions of Materials, ICMFM 96, N. Igata, Y. Hiki, I. Yoshida, and S. Sato, eds., University of Tokyo Press, Tokyo, Japan (September, 1996) pp. 293–300 (1996).
 17. D. D. Sieloff, S. S. Brenner, and M. G. Burke: Atom probe field-ion microscopy of conventionally cast & melt-spun nickel aluminide alloys containing boron and hafnium. *J. Phys.*, 47-C7:289–293 (1986).
 18. D. D. Sieloff, S. S. Brenner, and M. G. Burke: *FIM/Atom Probe Studies of B-Doped and Alloyed Ni₃Al*. Proc. High Temperature Ordered Intermetallic Alloys II, N. S. Stoloff, C. C. Koch, C. T. Liu, and O. Izumi, eds., Boston, MA (December 2–4, 1987) Materials Research Society, Pittsburgh, PA, 81:87–97 (1987).
 19. D. N. Sieloff, S. S. Brenner, and M.-J. Hua: *The Microchemistry of Grain Boundaries in Ni₃Al*. Proc. High Temperature Ordered Intermetallic Alloys III, C. T. Liu, A. I. Taub, N. S. Stoloff, and C. C. Koch, eds., Boston, MA (November 29–December 1, 1988) Materials Research Society, Pittsburgh, PA, 133:155–160 (1989).
 20. S. S. Brenner and M.-J. Hua: Grain boundary segregation of carbon and boron in Ni₃Al + B/C. *Scripta Metall.* 24:667–670 (1990).
 21. S. S. Brenner and M.-J. Hua: On grain boundary phases in B-doped Ni₃Al. *Scripta Metall.* 24:671–676 (1990).
 22. S. S. Brenner and M.-J. Hua: FIM/atom probe analysis of grain boundaries in B-doped Ni₃Al. *Scripta Metall.* 25:1271–1276 (1991).
 23. R. Jayaram and M. K. Miller: An atom probe study of grain boundary and matrix chemistry in microalloyed NiAl. *Acta Metall.* 42:1561–1572 (1994).
 24. A. J. Duncan, M. J. Kaufman, and M. K. Miller: Segregation of interstitial impurities in single-crystal NiAl. *Surface Sci.* 76/77:160–164 (1994).
 25. P. P. Camus, I. Baker, J. A. Horton, and M. K. Miller: Grain boundary chemistry in NiAl. *J. Phys.* 49-C6:329–333 (1988).
 26. R. Jayaram and M. K. Miller: An APFIM analysis of grain boundaries and precipitation in boron-doped NiAl. *Surface Sci.* 266:310–315 (1992).
 27. R. Jayaram and M. K. Miller: *An Atom Probe Field Ion Microscope Investigation of the Role of Boron in Precipitates and at Grain Boundaries in NiAl*. Proc. Structure and Properties of Interfaces in Materials, W. A. T. Clark, U. Dahmen, and C. L. Briant, eds., Boston, MA (December 2–5, 1991) Materials Research Society, Pittsburgh, PA, 238:445–450 (1992).
 28. R. Jayaram and M. K. Miller: *Characterization of Doped NiAl by Atom Probe Field Ion Microscopy*. Proc. High Temperature Ordered Intermetallic Alloys, V. Baker, R. Darolia, J. D. Whittenberger, and M. H. Yoo, eds., Boston, MA (November 30–December 3, 1992) Materials Research Society, Pittsburgh, PA, 288:355–360 (1993).
 29. R. Jayaram, C. T. Liu, and M. K. Miller: *An Atom Probe Investigation of the Influence of Trace Impurities on the Mechanical Behavior of NiAl*. Proc. Alloy Modeling and Design, G. M. Stocks and P. E. A. Turchi, eds., Pittsburgh, PA (October 18–20, 1993) The Minerals, Metals, and Materials Society, Warrendale, PA, pp. 283–290.
 30. M. K. Miller, R. Jayaram, and P. P. Camus: Grain boundary composition in NiAl. *Scripta Metall.* 26: 679–684 (1992).
 31. R. Jayaram and M. K. Miller: An atom probe characterization of carbon-doped NiAl. *Appl. Surface Sci.* 67:311–315 (1993).
 32. R. Jayaram and M. K. Miller: Direct observation of zirconium segregation to dislocations and grain boundaries in NiAl. *Scripta Metall. Mater.* 33:19–26 (1995).
 33. R. Jayaram and M. K. Miller: *Influence of Dislocation-Solute Interactions on the Mechanical Properties of Zirconium-Doped NiAl*. Proc. High Temperature Ordered Intermetallic Alloys, J. A. Horton, I. Baker, S. Hanada, R. D. Noebe, and D. S. Schwartz, eds., Boston, MA (November 28–December 1, 1994) Materials Research Society, Pittsburgh, PA, 364: 449–454 (1995).
 34. M. K. Miller, I. M. Anderson, and K. F. Russell: Precipitation and grain boundary segregation in molybdenum-doped NiAl. *Appl. Surface Sci.* 94/ 95:288–294 (1996).

35. M. K. Miller: Determination of the site occupation probability and the degree of order by APFIM. *J. Microsc.* 147:159–167 (1987).
36. M. K. Miller and J. A. Horton: Site occupation determinations by APFIM for Hf, Fe, and Co in Ni₃Al. *Scripta Metall.* 30:1125–1130 (1986).
37. M. K. Miller and J. Bentley: Comparison of site occupation determinations by APFIM and AEM. *J. Phys.* 47-C7:463–468 (1986).
38. K. Hono, H. Numakura, I. A. Szabó, A. Chiba, and T. Sakurai: Determination of the site preference of Cu and Ge in Ni₃Al. *Surface Sci.* 266:358–363 (1992).
39. K. Hono, A. Chiba, T. Sakurai, and S. Hanada: Determination of the site occupation probability of Cu in Ni₃Al by atom probe field ion microscopy. *Acta Metall.* 40:419–425 (1992).
40. H. Numakura, T. Yamada, M. Koiwa, I. A. Szabó, K. Hono, and T. Sakurai: An atom probe study of the site preference of Ge in Ni₃Al. *Defects Diffusion Forum* 95–98:869–874 (1993).
41. A. Menand, S. Chambrelaud, and C. Martin: Atom probe study of titanium base alloys: Preliminary results. *J. Phys.* 47-C2:197–202 (1986).
42. T. Hanamura, R. Uemori, and M. Tanino: Mechanism of plastic deformation of Mn-added TiAl L1₀-type intermetallic compound. *J. Mater. Res.* 3: 656–664 (1988).
43. M. Saga, R. Uemori, M. Tanino, and H. Morikawa: A combined AP-FIM/HREM approach to the characterization of microstructure in a Mn-added intermetallic compound. *Surface Sci.* 246:231–237 (1991).
44. Z. G. Liu, G. Frommeyer, and M. Kreuß: Field ion microscopy and atom probe investigations on two-phase intermetallic TiAl/Ti₃Al alloy. *Scripta Metall.* 25:1205–1210 (1991).
45. Z. G. Liu, G. Frommeyer, and M. Kreuß: Investigation on APBs and dissociation of super dislocations in TiAl by APFIM. *Philos. Mag. Lett.* 64:117–124 (1991).
46. Z. G. Liu, G. Frommeyer, and M. Kreuß: Microchemical and microstructural investigations on two-phase intermetallic TiAl/Ti₃Al alloys by field ion microscopy and atom probe. *Phys. Stat. Sol. (a)* 131:495–508 (1992).
47. Z. G. Liu, J. Wessemann, G. Frommeyer, and M. Kreuß: Evidence of (011) twins in γ -TiAl investigated by field ion microscopy. *Scripta Metall. Mater.* 33:627–631 (1995).
48. R. Uemori, T. Hanamura, and H. Morikawa: Oxygen scavenging of the α_2 phase in the TiAl intermetallic compound. *Scripta Metall.* 26:969–974 (1992).
49. A. Denquin, S. Naka, A. Huget, and A. Menand: Atom-probe investigation of the partitioning elements in two-phase $\gamma + \alpha_2$ TiAl-based alloys. *Scripta Metall.* 28:1131–1136 (1993).
50. S. C. Huang and E. L. Hall: *Microstructure and Deformation of Rapidly Solidified TiAl Alloys*. Proc. High Temperature Ordered Intermetallic Alloys III, C. T. Liu, A. I. Taub, N. S. Stoloff, and C. C. Koch, eds., Boston, MA (November 29–December 1, 1988) Materials Research Society, Pittsburgh, PA, 133:373–383 (1989).
51. V. K. Vasudevan, M. A. Stucke, S. A. Court, and H. L. Fraser: The influence of second phase Ti₃Al on the deformation mechanisms in TiAl. *Philos. Mag. Lett.* 59:299–307 (1989).
52. A. Huget and A. Menand: Atom-probe determination of interstitial element concentration in two-phase and single-phase TiAl-based alloys. *Appl. Surface Sci.* 76/77:191–197 (1994).
53. A. Menand, S. Huget, and A. Nerac-Pertaix: Interstitial solubility in γ and α_2 phases of TiAl-based alloys. *Acta Mater.* 44:4729–4737 (1996).
54. A. Nerac-Pertaix and A. Menand: Atom probe analysis of oxygen in ternary TiAl alloys. *Scripta Mater.* 35:199–203 (1996).
55. D. J. Larson and M. K. Miller: Microstructural characterization of $\alpha_2 + \gamma$ titanium aluminides. *Microsc. Microanal.* 3(Suppl. 2):701–702 (1997).
56. M. K. Miller, D. J. Larson, and K. F. Russell: *Characterization of Segregation in Nickel and Titanium Aluminides*. Proc. Second International Symposium on Structural Intermetallics, M. V. Nathal, R. Darolia, C. T. Liu, P. L. Martin, D. B. Miracle, R. Wagner, and M. Yamaguchi, eds., Champion, PA (September 21–25, 1997) The Minerals, Metals, and Materials Society, Warrendale, PA, pp. 53–62.
57. D. J. Larson, C. T. Liu, and M. K. Miller: Microstructural characterization of segregation and precipitation in $\alpha_2 + \gamma$ titanium aluminides. *Mater. Sci. Eng. A* 239–240:220–228 (1997).
58. D. J. Larson and M. K. Miller: Precipitation and segregation in $\alpha_2 + \gamma$ titanium aluminides. *Mater. Sci. Eng. A* 250:65–71 (1998).
59. H. Inui, K. Kishida, M. Kobayashi, M. Yamaguchi, M. Kawasaki, and K. Ibe: Compositional variations at TiAl-TiAl lamellar boundaries in binary and some ternary polysynthetically twinned TiAl. *Philos. Mag. A* 74:451–464 (1996).
60. D. J. Larson and M. K. Miller: *Solute Partitioning and Interfacial Segregation in TiAl-Based Alloys*. Proc. High Temperature Ordered Intermetallic Alloys VIII, E. P. George, M. Yamaguchi, and M. J. Mills, eds., Boston, MA (November 30–December 4, 1998) Materials Research Society, Pittsburgh, PA 552:KK2.9.1–KK2.9.6 (1999).
61. A. Menand, H. Zapolsky-Tatarenko, and A. Nerac-Pertaix: Atom-probe investigations of TiAl alloys. *Mater. Sci. Eng. A* 250:55–64 (1998).
62. S. Kim, G. D. W. Smith, S. G. Roberts, and A. Cerezo: Alloying element characterization in γ -based titanium aluminides by APFIM. *Mater. Sci. Eng. A* 250:77–82 (1998).
63. D. J. Larson, C. T. Liu, and M. K. Miller: The alloy-

- ing effects of tantalum on the microstructure of an $\alpha_2 + \gamma$ titanium aluminide. *Mater. Sci. Eng. A* 207:1–8 (1999).
64. P. J. Maziasz, C. T. Liu, and J. L. Wright: *Stability of Ultrafine Lamellar Structures During Aging in Two-Phase γ -TiAl Alloys*. Second International Symposium on Structural Intermetallics, M. V. Nathal, R. Darolia, C. T. Liu, P. L. Martin, D. B. Miracle, R. Wagner, and M. Yamaguchi, eds., Champion, PA (September 21–25, 1997) The Minerals, Metals, and Materials Society, Warrendale, PA, pp. 245–252.
 65. J. Wessemann, G. Frommeyer, and M. Kreuß: APFIM investigations on ordered γ -TiAl using single-layer detection method. *Appl. Surf. Sci.* 87/88:179–184 (1995).
 66. J. Wessemann, Z. G. Liu, G. Frommeyer, and M. Kreuß: APFIM investigations on the γ phase of TiAl alloys with additions of niobium and vanadium. *Phys. Stat. Sol. (a)* 148:K61–K63 (1995).
 67. S. C. Huang and E. L. Hall: *Characterization of the Effect of Chromium Additions to TiAl-Base Alloys*. Proc. Alloy Phase Stability and Design, G. Malcolm Stocks, D. P. Pope, and A. F. Giamei, eds., San Francisco, CA (April 18–20, 1990) Materials Research Society, Pittsburgh, PA, 133:381–386 (1991).
 68. S. Kim and G. D. W. Smith: AP-FIM investigation on γ -based titanium aluminides. *Mater. Sci. Eng. A* 239–240:229–234 (1997).
 69. S. C. Huang and E. L. Hall: *Structures and Properties of Gamma-TiAl Alloys Containing Interstitial Elements*. Proc. High Temperature Ordered Intermetallic Alloys IV, L. A. Johnson, D. P. Pope, and J. O. Stiegler, eds., Boston, MA (November 27–30, 1991) Materials Research Society, Pittsburgh, PA, 213: 827–832 (1991).
 70. R. V. Ramanujan, P. J. Maziasz, and C. T. Liu: The thermal stability of the microstructure of γ -based titanium aluminides. *Acta Mater.* 44:2611–2642 (1996).
 71. T. Nakano and Y. Umakoshi: Effect of boron addition on the plastic behavior of polysynthetically twinned crystals of TiAl. *Intermetallics* 2:185–191 (1994).
 72. D. J. Larson, C. T. Liu, and M. K. Miller: Boron solubility and boride compositions in $\alpha_2 + \gamma$ titanium aluminides. *Intermetallics* 5:411–414 (1997).
 73. D. J. Larson, C. T. Liu, and M. K. Miller: Tungsten segregation in $\alpha_2 + \gamma$ titanium aluminides. *Intermetallics* 5:479–482 (1997).
 74. H. Inui, M. H. Oh, A. Nakamura, and M. Yamaguchi: Room-temperature tensile deformation of polysynthetically twinned crystals of TiAl. *Acta Metall.* 40:3095–3104 (1992).
 75. D. J. Larson, M. K. Miller, M. Yamaguchi, and H. Inui: Atom probe field ion microscopy of polysynthetically twinned titanium aluminide. *Microsc. Microanal.* 4(Suppl. 2):102–103 (1998).
 76. D. J. Larson, M. K. Miller, M. Yamaguchi, and H. Inui: Atom probe field ion microscopy of polysynthetically twinned Zr-doped titanium aluminide. Proc. Gamma Titanium Aluminides 1999, Yong-Wong Kim, D. M. Dimiduk and M. H. Loretto, eds., San Diego, CA (February 28–March 4, 1999) The Minerals, Metals and Materials Society, Warrendale, PA, in press.
 77. K. Hono, E. Abe, T. Kumagai, and H. Harada: Chemical compositions of ultrafine lamellae in the water-quenched Ti-48Al alloy. *Scripta Mater.* 35: 495–499 (1996).
 78. H. Wood, J. M. Hyde, A. Cerezo, and G. D. W. Smith: Short range order and phase separation in Ti-Al alloys. *Mater. Sci. Eng. A* 250:83–87 (1998).
 79. H. Liew, G. D. W. Smith, A. Cerezo, and D. J. Larson: Experimental studies of the phase separation mechanisms in Ti-15 at.% Al. *Mater. Sci. Eng. A* 270:9–13 (1999).
 80. D. J. Larson and M. K. Miller: In-situ micro-twinning of TiAl in the field ion microscope. *Mater. Sci. Eng. A* 250:72–76 (1998).
 81. D. J. Larson and M. K. Miller: Atom probe field ion microscopy of titanium aluminides. *Microsc. Microanal.* 4(Suppl. 2):100–101 (1998).

Received October 1998; accepted December 1998.